Heliyon 9 (2023) e20144

Contents lists available at ScienceDirect

Heliyon

journal homepage: www.cell.com/heliyon

Development of double crosslinked sodium alginate/chitosan based hydrogels for controlled release of metronidazole and its antibacterial activity

Zerihun Feyissa *, Gemechu Deressa Edossa, Neeraj Kumar Gupta, Defaru Negera

Department of Applied Chemistry, School of Applied Natural Science, Adama Science and Technology University, P.O. Box 1888, Adama, Ethiopia

ARTICLE INFO

Keywords:
Sodium alginate
Chitosan
Metronidazole
Drug release
Swelling

ABSTRACT

Double network sodium alginate/chitosan hydrogels were prepared using calcium chloride ($CaCl_2$) and glutaraldehyde as the crosslinking agents by the ionotropic interaction method for controlled metronidazole release. The effect of polymer ratios and $CaCl_2$ amount is investigated by the developing porosity, gel fraction, and extent of swelling in simulated physiological fluids. Interaction between the polymers with the formation of crosslinked structures, good stability, phase nature, and morphology of the hydrogels is revealed by Fourier-transform infrared spectroscopy, thermogravimetric analysis, X-ray diffraction, and scanning electron microscopy. A sodium alginate/chitosan hydrogel (weight ratio of 75:25) crosslinked with two percent $CaCl_2$ is chosen for the in-situ loading of 200 mg of metronidazole. The drug release kinetics using different models show that the best-fit Korsmeyer-Peppas model suggests metronidazole release from the matrix follows diffusion and swelling-controlled time-dependent non-Fickian transport related to hydrogel erosion. This composition displays enhanced antimicrobial activity against *Staphylococcus aureus* and *Escherichia coli*.

1. Introduction

The development of controlled drug delivery systems (CDDSs) emphasizes on drug administration that matches physiological requirements through a continuous release of the drug at predetermined rates for an extended period of time to attain the right therapeutic effects [1]. With the conventional formulations, the drug blood level increases after each administration of the drug reaches the upper dosage, and then falls below the effective limit till the next administration [2]. Whereas, CDDSs regulate drug delivery keep drug concentration within optimal and effective range, increase the efficacy of a drug, minimize side effects, fewer dosing frequency, improve patient compliance, enhance the solubility of lipophilic drugs, increase bioavailability, reduce the development of resistant bacteria, and decrease the wastage of highly water soluble drugs which need slower and extended time of release [3,4]. On this account, hydrogels emerged as promising polymeric materials for drug delivery systems, because of their ease of processing, easily controllable physical and chemical properties such as excellent biocompatibility, bio-adhesive, excellent hydrophilic nature, and capability of swelling [5].

* Corresponding author. Department of Applied Chemistry, School of Natural Science Adama Science and Technology University P.O. Box 1888, Adama, Ethiopia.

E-mail addresses: zerefeyem@gmail.com (Z. Feyissa), gemechu.deressa@astu.edu.et (G.D. Edossa), kumerneerej@gmail.com (N.K. Gupta), negaradefaru@gmail.com (D. Negera).

https://doi.org/10.1016/j.heliyon.2023.e20144
Received 5 June 2023; Received in revised form 8 September 2023; Accepted 13 September 2023
Available online 16 September 2023

Hydrogels are crosslinked hydrophilic polymers with 3D network structures capable of absorbing large amounts of water and physiological fluids, without crumbling and forming swollen state [6]. Hydrogels can undergo significant changes in volume when exposed to various external environmental stimuli including temperature, pH, ionic strength, and glucose concentration [7]. Hydrogels are often able to be tailored for specific drug release rates and designed to degrade for ease of their removal from the body [8]. Because of their superior biocompatibility, hydrogels are considered ideal drug carriers.

Crosslinked hydrogels can be synthesized by chemical or physical interactions. Chemical crosslinking of hydrogel is usually based on the nature bonds between polymer and crosslinking agent, which creates a stronger, more resistant polymer matrix to heat, wearing and attack by various solvent media. A specific functional group of crosslinkers affects the nature of hydrogel specifically its mechanical strength. The physical crosslinking approach of hydrogel preparation involves non-covalent interactions including ionic interactions, hydrogen bonding, and the crystallization process [9]. As the physical crosslinking method does not require multifunctional crosslinkers, it does not associate with toxicity and hence, further purification is also not required. The physical crosslinks are not permanent and yield reversible hydrogel products [10]. Biocompatible and biodegradable natural polymers (e.g., alginate, chitosan, guar gum, cellulose, and collagen) and synthetic polymers such as poly (vinylpyrrolidone), poly (vinyl alcohol), poly (ethylene oxide), polyacrylamide, etc. have been used to develop hydrogels for biomedical applications [11–15].

Chitosan is a natural polysaccharide consisting mainly randomly distributed residues of β (1 → 4) linkage of 2-amino-2-deoxy-D-glucose and 2-acetamido-2-deoxy-D-glucose interconnected structural units [16]. It is produced by the alkaline deacetylation of chitin and has two functional groups, the primary amine (–NH_2) and hydroxyl (–OH) groups, in its structure, which act as electron donors and help crosslink CS with other polymers [17]. Due to its cationic nature (R–NH_3^+), chitosan based hydrogels are soluble in dilute acidic medium and hence exhibit poor mechanical strength [18]. To this end, modification of the chitosan structure by crosslinking with other biocompatible natural polymers such as sodium alginates is an effective approach to improve its mechanical strength to make suitable material for use in CDDSs.

Sodium alginate (SALG) is also a polysaccharide comprising different proportions of α-(1 → 4)-linked L-guluronic acid (G) and β-(1 → 4)-linked β-mannuronic acid (M) with carboxyl group (-COO^-) in its chain [19]. It is a hydrophilic and linear natural polymer produced from brown algae [20]. SALG has outstanding gel producing behavior in the presence of divalent cations (e.g., Ca^{2+}) by replacing the sodium ions to form networked microbeads [21]. The presence of anionic carboxyl functional group (-COO^-) and its pH-dependent solubility, super biocompatibility, bioadhesive, and biodegradability have made SALG an important candidate for CDDSs [22,23].

However, SALG alone dissolves in intestinal fluids resulting in the disintegration of the crosslinked structure leading to an uncontrollable drug release [24,25]. For this reasons, hydrogels produced by single crosslinking of SALG with other biocompatible polymers (e.g., chitosan) have been used for CDDSs applications [15,26]. Chitosan/alginate hydrogel composite for controlled release of deferoxamine was reported in previous study [27]. It has been reported that ibuprofen loaded chitosan/sodium alginate nanoparticle showed good an in vitro drug release behavior [28]. However, despite its advantages, owing to weak physical interactions SALG and CS based hydrogels display relatively poor mechanical stability in physiological fluids and disintegrate after swelling [29,30]. To overcome the above mentioned drawbacks of SALG/CS based hydrogels, double-crosslinking using different crosslinking agents is needed to produce hydrogels with improved properties suitable for slow drug release applications. Only few studies have reported double crosslinked SALG/CS hydrogels for controlled drug release applications. It has been suggested that double crosslinked chitosan/sodium alginate hydrogels had promising application for the controlled release of doxorubicin hydrochloride [23]. Multilayered alginate/CS for oral administration of cranberry fruit extract has been reported [31]. To the best of our knowledge, there is no previous study report on double-crosslinked SALG/CS hydrogel incorporating metronidazole for oral administration application.

Metronidazole (MTZ) is an antibiotic and antiprotozoal drug which is on the list of essential medicines by WHO [32]. It is available as immediate release in capsule and tablet forms, and no formulation for sustained and controlled release form currently. The conventional administration of MTZ directly to the targeting site is associated with some side effects. The commonly reported side effects include anorexia, dizziness, nausea, peripheral neuropathy, vomiting, and epigastric pain. The presence of high concentrations of MTZ in the saliva cause mouth dryness and resistant bacteria strains emergence are reported [33,34]. Thus, to decrease the dosing frequency, and mitigate the side effects developing a controlled release system for MTZ delivery is needed.

This present study reports the development of SALG and CS based double crosslinked hydrogel systems via the ionotropic interaction method using $CaCl_2$ and glutaraldehyde crosslinkers for the controlled release of metronidazole (MTZ). In order to achieve this goal, the hydrogel production was designed in two steps. In the first step single crosslinked hydrogel systems with different polymer ratios (SALG:CS) were produced using fixed $CaCl_2$ crosslinker. These hydrogels were then socked into enough glutaraldehyde crosslinker to obtain the double crosslinked hydrogels. In the second step, the optimal polymer ratio based on the swelling ratio in simulated physiological fluids was used to evaluate the effect of $CaCl_2$ concentration to optimize a formulation suitable for drug delivery applications. The hydrogels were characterized by FTIR, XRD, SEM, and TGA. Further, the hydrogels were analyzed for swelling behavior and biodegradation. The drug release profile and the kinetics of release were established using a UV–Vis spectrophotometer at 322 nm and different kinetic models. The antimicrobial activity was determined for the optimal MTZ loaded hydrogel.

2. Experimental

2.1. Materials

CS (≥75% deacetylated having bulk a density of 0.15–0.3 g/cm^3 and viscosity >200 Cp) was purchased from Sisco Research Laboratory Pvt. Ltd (India). Sodium alginate (food grade, purity 91%), calcium chloride ($CaCl_2$, 99%, AR), glutaraldehyde solution

(grade-II 25% in water), glacial acetic acid ($C_2H_4CO_2$, purity 99.75%, AR), and ethanol (C_2H_6O, 97.6%, AR), sodium hydroxide (NaOH, 99%, AR) and hydrochloric acid (HCl, 37%, AR) were all purchased from Loba Chemie Pvt. Ltd (India). Sodium chloride (NaCl, 99.5%, AR), potassium chloride (KCl, 99.5%, AR), dibasic sodium phosphate (Na_2HPO_4, 99.5%, AR), potassium phosphate monobasic (KH_2PO_4, 99.5%, AR) are used for the preparation of the phosphate buffer solution (PBS) and Mueller Hinton Agar (MHA) [OXOID CM0337] were purchased from Sigma-Aldrich. Pristine MTZ (β-lactam antibiotic) drug was provided by Ethiopian Pharmaceuticals Manufacturing Sh. Co. (EPHARM) Ethiopia. Double distilled deionized water (DDW) was used all through this study.

2.2. Synthesis of SALG/CS hydrogels

The SALG/CS hydrogels were prepared by ionotropic synthesis method [23]. To prepare CS solution the composition of the polymer (Table 1) was dissolved in 200 mL aqueous solution of 2% (v/v) acetic acid. A separate SALG solution was prepared by dissolving the requisite amounts (Table 1), in 200 mL of DDW. The two solutions were then blended using an overhead stirrer at speed of 700 rpm for 90 min at room temperature. Under stirring, aqueous solution of 1.0 M NaOH was added to adjust the pH of the SALG/CS solution to pH 5 using. This blend was added into a separate 200 mL of 2% (w/v) $CaCl_2$ aqueous solution under constant stirring at 700 rpm dropwise at 60 drops/min. Subsequently, standing for over 4 h, the solution blend was washed with DDW and filtered. Then, the microbeads formed were soaked in 25% (w/v) glutaraldehyde solution for 48 h. The double crosslinked microbeads were then transferred into glass Petri dishes plates and dried in a vertical thermostatic shaking incubator (LFZ-TSI series, China) at 40 °C. The dried hydrogels were stored in a desiccator to avoid moisture adsorption till required.

The hydrogel bead, B1 (determined as optimal based on the swelling ratio in simulated physiological fluids) was used to evaluate the effect of the cationic crosslinker concentration ($CaCl_2$) by varying the concentration shown in Table 2.

2.3. Synthesis of MTZ loaded SALG/CS hydrogel beads

200 mg of MTZ was loaded into the hydrogel B1–C1 (determined as having the optimal swelling capacity in the simulated physiological fluids). CS solution was prepared by dissolving 2 g of CS in 200 mL of aqueous solution of 2% (v/v) acetic acid. Then, 100 mL aqueous solution of MTZ drug was mixed with the CS solution (B1) while stirring by overhead stirrer at room temperature. 6 g of SALG was dissolved separately in 200 mL of DDW. The two separate solutions were then mixed and stirred using an overhead stirrer at 700 rpm for 80 min at room temperature. Afterward, the same steps were repeated as for the preparation of SALG/CS hydrogel beads.

2.4. Preparation of simulated physiological fluids

Three simulated physiological fluids of different pH including gastric fluid (SGF), intestinal fluid (SIF), and colon fluid (SCF) were produced using a previously reported procedure [35]. To prepare SGF, 2 g NaCl and 7 mL of 0.2 N HCl were mixed in DDW to a final volume of 1L solution with the pH adjusted to 1.2 ± 0.1. To prepare SIF with pH 6.8, KH_2PO_4 (6.8 g) and NaOH (0.94 g) were mixed in 1 L DDW and then pH was adjusted using 1 M NaOH. To prepare SCF with pH 7.4, 8 g NaCl, 0.2 g KCl, 1.15 g Na_2HPO_4, and 0.2 g KH_2PO_4 were mixed in DDW to a final volume of 1 L and the pH adjustment of the physiological fluid made using 1 M HCl/1 M NaOH.

3. Characterization

3.1. Swelling behavior

To evaluate the effects of polymer ratio (Table 1) and crosslinker concentration (Table 2) on the pH responsive nature of the synthesized hydrogels, the swelling ratio of the hydrogel compositions was determined gravimetrically by soaking a pre-weighed (W_i) microbeads in the prepared simulated physiological fluids (SGF, SIF, and SCF) and incubated in the vertical thermostatic shaking incubator at 37.2 °C mixing at 100 rpm [36]. The hydrogel samples were removed from the simulated physiological fluids after time intervals of 10, 30, 60, 90, 120, 150, 180, 210, and 240 min, gently wiped between Whatman filter paper No.2 and weighed (W_t). This step was repeated until the constant mass of the hydrogel sample was determined. The calculation of the swelling ratios was performed by using eq. (1).

$$\text{Swelling ratio } (\%) = (\text{Wt} - \text{Wi}) / \text{Wi x } 100 \quad (1)$$

Table 1
Composition of SALG/CS hydrogel beads.

Hydrogel sample code	SALG/CS wt. % ratio (Total polymer mass 8 g)		$CaCl_2$ Concentration (%)
	SALG	CS	
B1	75	25	2
B2	67	33	2
B3	50	50	2
B4	33	67	2
B5	25	75	2

Table 2
Hydrogel B1 modified by varying the concentration of $CaCl_2$.

Hydrogel sample code	SALG/CS wt. % ratio (Total polymer mass 8 g)		$CaCl_2$ Concentration (%)
	SALG	CS	
B1–C1	75	25	2
B1–C2	75	25	4
B1–C3	75	25	6
B1–C4	75	25	8
B1–C5	75	25	10

3.2. Porosity

The ethanol solvent replacement method was used for porosity measurement [37]. The porosity of the hydrogels (Table 1) and (Table 2) was determined using a stoppered 25 mL beaker by taking the weight of the empty stoppered beaker as W_1. A pre-weighed hydrogel sample (W_h) was placed into the beaker and 20 mL of ethanol (C_2H_5O) was added to the hydrogels in the beaker, and the total weight (W_2) was recorded. The hydrogel samples were removed from the beaker after 24 h standing and the weight of the remaining components determined (W_3). It is assumed that the volumes of the ethanol full in the hydrogel pores were taken as the porosity of the hydrogels. The calculation of the porosity of the hydrogel samples was performed by using eq. (2). In the equation, ρ_e, is the density of absolute ethanol.

$$\text{Porosity } (\%) = (W2 - W3 - Wh) / (W1 - W3 + 20\rho e)\ x100 \quad (2)$$

3.3. Fourier-transform infrared spectroscopy (FTIR)

The FTIR data of the pristine CS, SALG, MTZ, unloaded hydrogels (B1–C1, B1–C2, B1–C3, B1–C4, and B1–C5) and the drug loaded hydrogel MTZ-B1-C1 were recorded by an FTIR spectrometer (Alpha-T, Bruker, Germany). The microbeads samples were ground and compressed with KBr to obtain pellets. The FTIR measurements were performed at a scanning rate of 120 scans per minutes in the wavelength range of 4000-500 cm^{-1}, with resolution of 4 cm^{-1}.

3.4. X-ray diffraction (XRD)

X-ray diffraction of pristine CS, SALG, MTZ, unloaded hydrogels (B1–C1, B1–C2, B1–C3, B1–C4, and B1–C5) and the drug loaded hydrogel MTZ-B1-C1 were obtained from an XRD-7000, SHIMADZU, Japan with CuKα radiation source (1.5406° A), steps at a scanning rate of 2θ 3°/min, applied voltage of 40 kV and current of 30 mA in the 2θ range 5°–40° at room temperature.

3.5. Thermogravimetric analysis (TGA)

TGA of pristine SALG, CS, MTZ, unloaded hydrogels (B1–C1, B1–C2, B1–C3, B1–C4, and B1–C5) and the drug loaded hydrogel MTZ-B1-C1 was carried out using a DTA-TGA instrument (ATAT 2012, BJ HENVEN) at a heating rate of 15 °C per minute under nitrogen flow of 20 mL min^{-1} and within the temperature range of room temperature to 650 °C.

3.6. Gel fraction

The gel content of the prepared hydrogel microbeads (Table 1) and (Table 2) was determined by immersing a measured weight (Wi) of the sample in DDW for 48 h at room temperature to remove out the non-crosslinked polymer fractions [38]. The extracted hydrogels were filtered, washed copiously with deionized water, and dried at 60 °C till constant weight (W_f) was obtained. Eq. (3) was used to calculate the percentage gel content of the hydrogel microbeads.

$$\text{Gel fraction } (\%) = Wf/Wi\ x\ 100 \quad (3)$$

3.7. In vitro biodegradation assay

Pre-weighed (W_i) of the unloaded hydrogels (B1–C1, B1–C2, B1–C3, B1–C4, and B1–C5) were immersed in SCF (pH = 7.4) and incubated in vertical thermostatic shaking incubator at 37.2 °C under shaking at 80 revolutions per minute for 30 days. After an interval of 2–3 days, the hydrogel microbeads were taken out from the buffer solution, gently wiped out using clean filter paper (Whatman filter paper No.2) to eradicate the surface solution, and weighed (W_f) was recorded. The immersion solution was replaced with fresh SCF and incubated at the same temperature. Eq. (4) [37], was used to calculate the weight loss percentage.

$$\text{Weight loss } (\%) = [(Wt - Wi) / Wi]x\ 100 \quad (4)$$

3.8. Field emission scanning electron microscopy (FESEM)

FESEM (ApreoS, Thermo Fisher Scientific, Singapore) was used to examine the morphology of the unloaded hydrogels (B1–C1, B1–C2, B1–C3, B1–C4, and B1–C5) and the drug loaded hydrogel MTZ-B1-C1. Before imaging, the samples were coated with a thin film of gold.

3.9. In vitro MTZ release

The in vitro cumulative MTZ percentage release from the hydrogel MTZ-B1-C1 was determined by immersing the hydrogel microbeads in 50 mL of the simulated physiological fluids (SGF, pH 1.2; SIF, pH 6.8; and SCF, pH 7.4) under continuous shaking at 100 rpm at 37.2 °C [39]. Then, after time intervals of 1, 2, 3, 4, 5, 6, 7, 8, 9, 10, 11, 12, 13, 14, 15, and 24 h, the supernatant was withdrawn and replaced with fresh simulated physiological fluids. Absorbance measurement was performed using a UV–visible spectrophotometer (Maalab Scientific Equipment Ltd., India) at a wavelength of 322 nm. The released drug concentration was determined in triplicate against a calibration curve derived from standard solutions of MTZ (0.5, 2, 4, 6, 8, 10, 12 μg/liter)). Eq. (5), was used to calculate the percentage cumulative amount of MTZ released.

$$\text{Cumulative release } (\%) = \text{Ct/Ci x } 100 \quad (4)$$

where, C_t is the quantity of MTZ released at time t and C_i is the quantity of MTZ loaded into the SALG/CS hydrogel.

3.10. Drug release kinetics

The following kinetic models such as zero-order, first-order, Higuchi, and Korsmeyer-Peppas were fitted by in vitro MTZ release data to evaluate the kinetics and the mechanisms of MTZ from the SALG/CS hydrogel.

3.11. Antibacterial activity test

The antibacterial activity of MTZ-B1-C1 hydrogel was tested using inhibition zone method against gram-positive *Staphylococcus aureus (ATCC25923)* and gram-negative bacteria *Escherichia coli* (ATCC25922). The test was carried out in Mueller Hinton Agar (MHA, OXOID CM0337] medium. The sterilized agar media was dispensed into Petri plates and solidified. Freshly preparedmicroorganism cultures (1×10^8 CFU mL^{-1}, CFU, colony-forming units) were evenly apportioned on the surface of the solidified media. As soon as UV

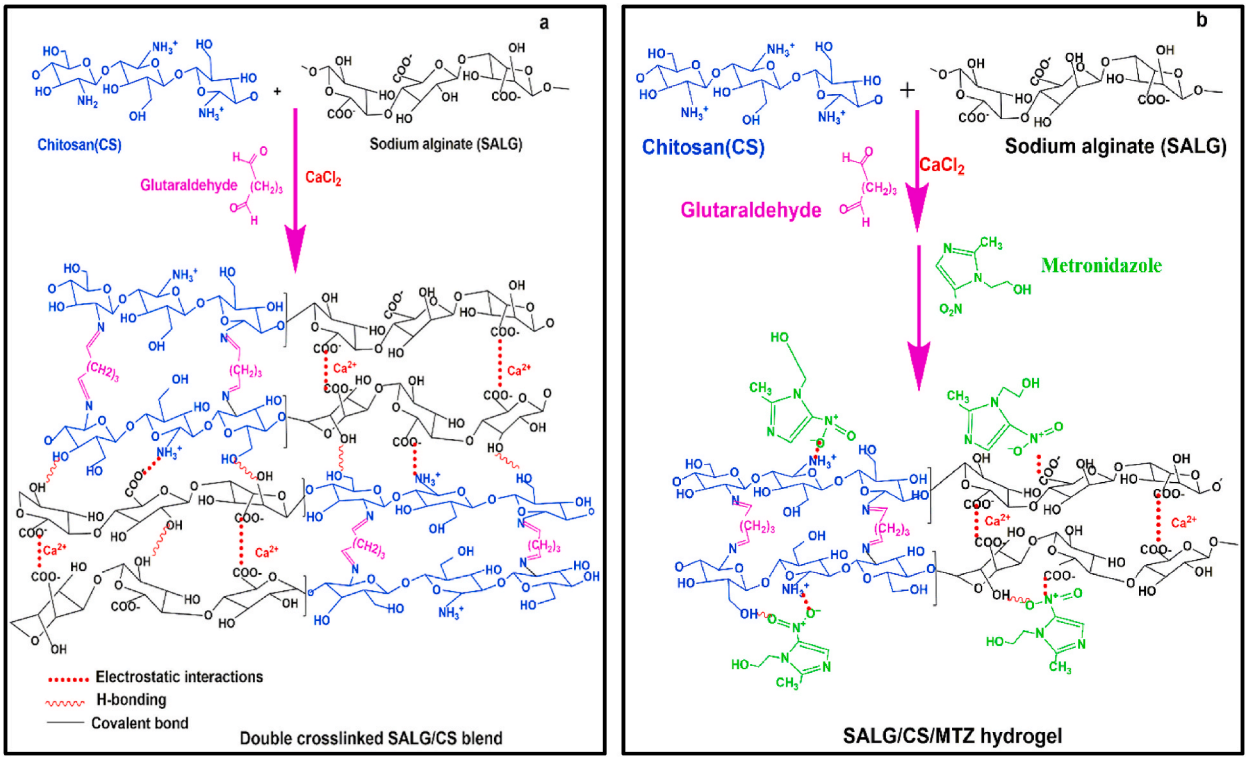

Fig. 1. (a, b). Schematic diagram indicating interactions of (a) CS and SALG polymers (b) CS, SALG and MTZ via glutaraldehyde crosslinker.

rays sterilized hydrogel, MTZ-B1-C1 it waspositioned on the agar nutrient in the plates that contained 20 μL of bacteria cell suspension. Upon incubation at 37 °C for 24 h, the plates were appraised for an inhibition zone. On the plate medium, a clear zone surrounding the sample indicated resistance against the bacteria. A ruler measured the zone, describing the region as the inhibition zone. The hydrogel B1–C1 was used as the negative control and the pristine MTZ as the positive control.

3.12. Statistical analysis

The statistical data analysis and figures were done using origin 2021b version software (Origin Lab Corporation, USA). All experiments were performed in triplicate and the data are expressed as mean ± standard deviation (SD).

4. Results and discussion

Double-crosslinked SALG/CS hydrogels with different ratios of the polymers using $CaCl_2$ and glutaraldehyde crosslinking agents were successfully prepared. The possible polymer-polymer and polymer-drug interaction mechanisms are shown in Fig. 1(a, b). Glutaraldehyde crosslinks the amino (-NH_2) end of CS chains through covalent bonding [37], and SALG chains are crosslinked by electrostatic interactions between the Ca^{2+} ions and the anionic alginate carbonyl ends (–COO–) forming an "egg-box" polymer networks by replacing the Na^+ [40]. The –COO– ends of SALG also interact with the cationic amino groups (-NH_3^+) of CS chains via electrostatic interactions [41]. The distinct inter-chain interactions between the polymer components resulted in the formation of denser double crosslinked interpenetrated networks. Similarly, MTZ, which is a hydrophilic drug is incorporated into the interpenetrated networks through different physical interactions, such as electrostatic and hydrogen bonding between polar groups of the drug and the polymer chains. The possible interaction mechanisms between SALG and CS have been reported in the literature [42,43]. In the current study, the proposed chemical and physical interactions between the polymer components and the drug are further confirmed by FTIR analysis.

4.1. Swelling behavior

The swelling of hydrogels owing to the absorption of physiological fluids helps the penetration of a drug into the hydrogel matrices and, in turn, leads to the diffusion of the drug providing the controlled drug release properties of the hydrogels. Fig. 2a-c shows the swelling ratios of B1 to B5 hydrogels (Table 1) in SGF (pH 1.2), SIF (pH 6.8), and SCF (pH 7.4). It is apparent that the swelling behavior of the SALG/CS hydrogels is varied based on the pH of the simulated physiological fluids and the composition of the polymers. In acidic medium (SGF), hydrogel B1 (SALG/CS wt.% 75/25) shows the lowest swelling ratio of ca. 84% compared to hydrogel B5 (SALG/CS wt.% 25/75), which has the highest swelling ratio of ca. 121%. This implies that SALG is stable in an acidic media, and as the CS wt.% increases, so does the swelling ratio, which is also confirmed by the swelling ratios of B2 to B4 hydrogels. In hydrogels B1 to B5, the ionic interaction between the ammonium cations (NH_3^+) in CS and –COO− groups present in SALG in SGF contribute to the reduction in

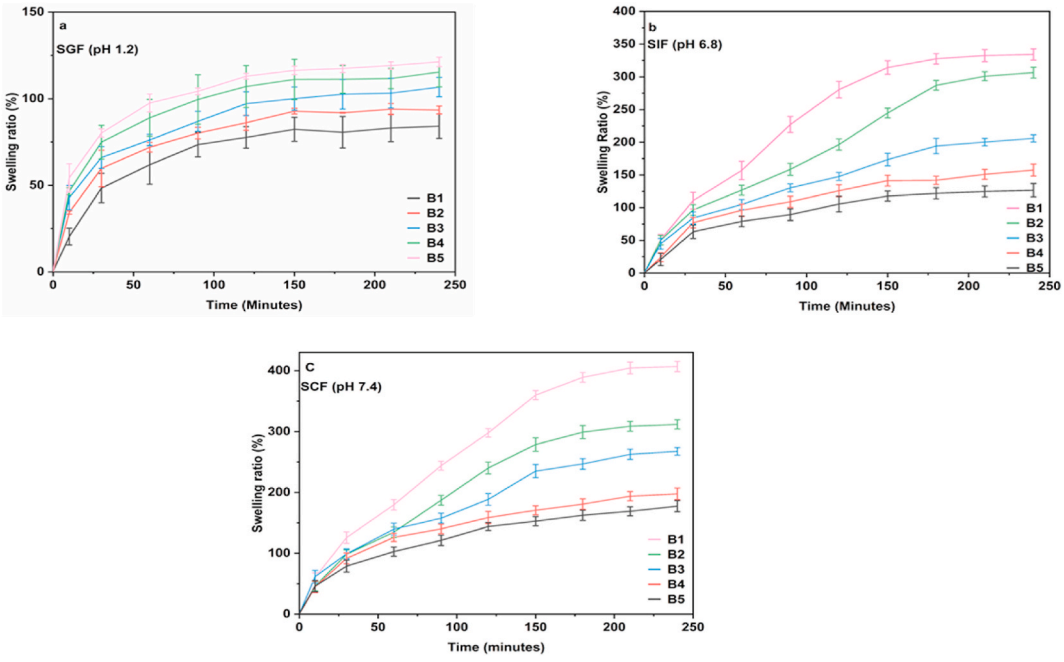

Fig. 2. (a–c). Swelling ratio of hydrogel beads B1to B5 in (a) SGF (b) SIF (c) SCF.

the swelling ratio. As the CS wt.% increases, so do the degree of ionic interaction and crosslinking between CS and SALG, resulting in more rigid networks [23].

The swelling degree of the hydrogel microbeads in the physiological fluids, irrespective of pH, can be divided into three time-dependent zones. In SGF, during the first time zone of 30 min, there is rapid uptake of SGF; in the second time zone, between 30 and 120 min, the uptake gradually slows down, and in the third time zone, between 120 min and 240 min, the uptake begins to taper towards equilibrium. This infers the stability of SALG in acidic media. However, the observed trend of swelling with increasing CS wt. % in SGF is reversed as the pH increases, i.e., in SIF and SCF.

Hydrogel B1 now shows the highest swelling ratio of ca. 334% and ca. 407%, respectively, compared to the swelling ratios of ca. 128% and ca. 177%, respectively, for hydrogel B5. This shows the pH responsiveness of the hydrogels. Other hydrogels (B2 to B4) also show similar responses with increased pH of the simulated physiological fluids. In SIF, the swelling behaviour of the hydrogels is divided into three time-dependent zones. Fluid uptake is rapid in the first time zone spanning the first 30 min; in the second time zone, beginning from 30 min to ca. 180 min, fluid uptake is gradual; and from 180 min to 240 min, the uptake tapers towards equilibrium.

The swelling behaviour of the hydrogel microbeads in SIF and SCF indicates that as the SALG wt.% increases, swelling increases, and CS attribute to the structural integrity of the hydrogel networks. The results show that among the hydrogels B1 to B5, hydrogel B1 could be a potent composition for possible MTZ loading and release based on its swelling behaviour, i.e., the low swelling ratio in SGF and increasing swelling in SIF and SCF. Thus, this composition was further studied for the consequence of varying the $CaCl_2$ amount on swelling to confirm the choice. Fig. 3a-c displays the swelling behaviour of hydrogels B1–C1 to B1–C5 as a function of increasing $CaCl_2$ concentration from 2% to 10% in SGF, SIF, and SCF. It is seen that while a similar trend of increasing swelling ratio with pH as for the hydrogel B1 is obtained in all three physiological fluids, there is a reduction in the swelling ratio with increasing concentration of $CaCl_2$. The obtained extent of swelling reflects the crosslinked network density, which increases with $CaCl_2$ concentration [44]. Due to this, the hydrogels become more compact and rigid, and the extent of swelling decreases [40,45].

4.2. Porosity

Porosity in hydrogels is among the critical physical features for their application as CDDSs [46]. The porosity of the hydrogels B1 to B5 is shown in Fig. 4a. It is seen that with an increase in the content of CS from 25 wt% (hydrogel B1) to 75 wt% (hydrogel B5), the porosity decreases from ca. 92% to ca. 75%, respectively. The reduction in porosity is attributed to glutaraldehyde crosslinking of CS chains resulted in the formation of acetal and Schiff base –OH and $–NH_2$ groups which are otherwise free. The modification in the structural arrangements of the polymer chains arising from crosslinking reduces the free space within the matrices of the hydrogels

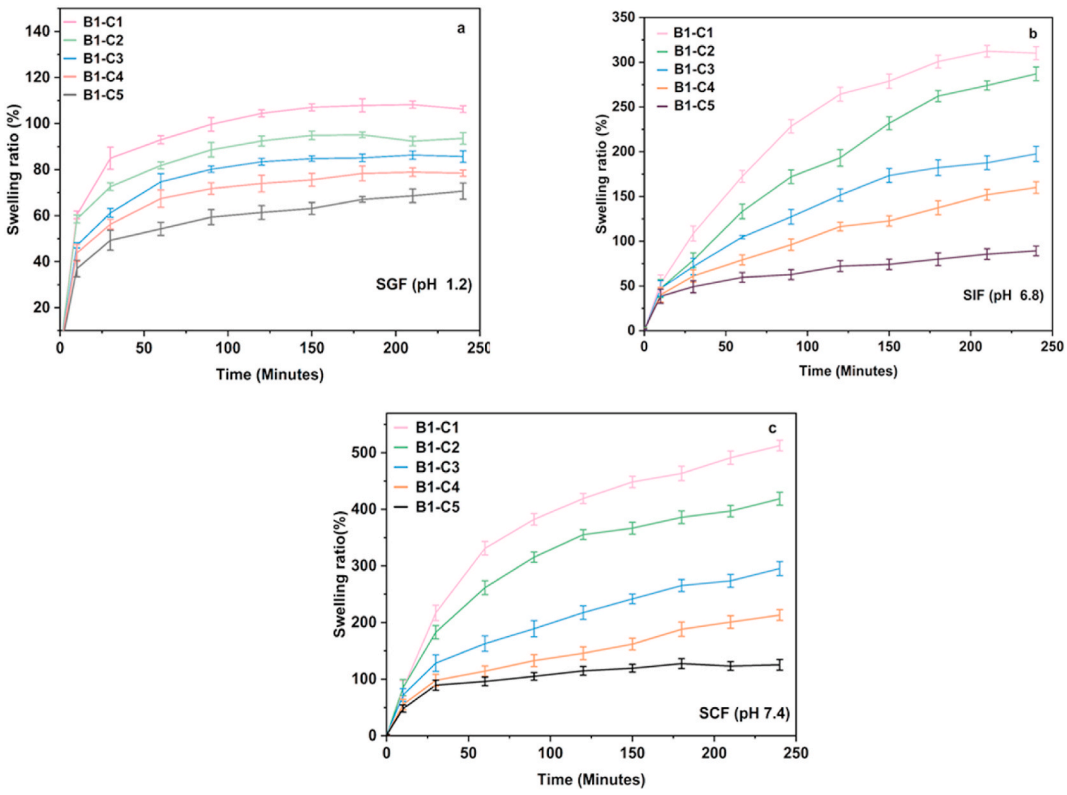

Fig. 3. (a–c). Swelling ratio of hydrogel bead B1 with increasing CaCl2 content in (a) SGF (b) SIF (c) SCF.

leading to a reduction in porosity [47].

The variation in porosity of the SALG/CS hydrogels B1–C1 to B1–C5 as a function of the $CaCl_2$ ionic crosslinking agent concentration is shown in Fig. 4b. The figure shows that the porosity of the hydrogels decreases proportionally to the crosslinking agent concentration, with the highest porosity of ca. 87% obtained for the hydrogel B1–C1 with a 2% crosslinker concentration and the lowest of ca. 69% for the hydrogel B1–C5 with 10% crosslinking agent. This implies the formation of smaller pores with increasing crosslink density of the hydrogels. Based on the above results, hydrogel B1–C1 was selected for the loading of MTZ.

4.3. Fourier-transform infrared spectroscopy (FTIR)

Fig. 5a shows the FTIR spectra of SALG and CS. SALG shows a broad range band between 3000 and 3700 cm^{-1} assigned to the stretching vibrations of O–H groups. The stretching vibrations C–H (aliphatic) are at 2920 cm^{-1}; C═O vibration (asymmetric and symmetric); COO- stretching are at ca. 1595 cm^{-1} and ca. 1394 cm^{-1} respectively. The stretching vibration of C–O is observed at ca. 1287 cm^{-1}. The small band at ca. 1084 cm^{-1} is related to the stretching vibrations of C–O, C–C, and COC bonds. Besides, the strong band at 1017 cm^{-1} is attributed to C–C and COC bond vibrations [48]. The band at ca. 816 cm^{-1} is assigned to Na–O [41].

CS shows a broad band of strong intensity between 3700 and 3000 cm^{-1}, attributed to the O–H groups and the N–H bonds of the primary amine groups overlapping stretching vibrations. The bands at 2920 and 2851 cm^{-1} are assigned to the stretching of the C–H of the methyl (–CH3) groups and alkyl (–CH2–) chains [49]. The presence of chitin is clearly observed by the amide carbonyl peak at 1600–1800 cm^{-1} because of the incomplete deacetylation of chitosan. Amides I, II, III, and N–H out-of-plane vibration are observed at ca. 1638, 1554, 1315, and 605 cm^{-1} respectively [50,51]. Bands at 1418 and 1381 cm^{-1} are due to the methyl (CH_3) symmetrical deformation mode, and those conforming to the saccharide structure of CS are at 1150 and 897 cm^{-1} [52].

Fig. 5b shows the spectra of the hydrogels B1–C1 to B–C5 as a function of the content of the polymers. The Na–O peak characteristic of sodium alginate at ca. 816 cm^{-1} is present in all the hydrogels. It is seen from Fig. 5a and b the carbonyl (C═O) peak in the SALG spectrum (1595 cm^{-1}) shifts to 1634 cm^{-1}. This shift of the band to a higher wavenumber is at due to CS present in the hydrogels. The amide I (C═O) and amide II (C–N) peaks of CS at 1642 cm^{-1} and 1554 cm^{-1} are replaced by this peak due to the interaction of the carboxylic groups (–COO–) present on alginate chain adjacent accumulates into a network matrix and the peak of the amino group at 1173 cm^{-1} disappears. These observations infer the presence of interactions between the anionic alginate carbonyl groups and cationic amino groups of CS (Fig. 1a) [41].

Fig. 5c shows the FTIR spectra of pristine MTZ and MTZ-B1-C1 hydrogel. From the figure, it is observed that the spectrum of pristine MTZ shows an absorption band at 3221 cm^{-1} (O–H stretching vibrations), band at and 3099 cm^{-1} (imidazole, C═C–H, stretching vibration) [53,54], and the C–H of the methyl (–CH_3) groups and alkyl (–CH_2–) chains stretching vibrational bands are at 2937 and 2853 cm^{-1} [55].

The bands at 1807 cm^{-1} and 1473 cm^{-1} are due to N–O stretching (asymmetric and symmetric asymmetric) of NO_2 bonds [56]. The bands at 1535 and 1367 cm^{-1} (nitroso, N–O stretching), 1263 cm^{-1} (–C═C– stretching), 1186 cm^{-1} (–C═N stretching), 1072 cm^{-1} (C–O stretching), 824 cm^{-1}(C–H stretching) [16,53]. The observed FTIR spectra in MTZ-B1-C1 at 1645 cm^{-1} (C═O stretching), at 1110 cm^{-1} (C–H of benzene ring deformation vibration), and 1381 cm^{-1} (-CH_2 bond bending vibrations). The newly appeared peak at 1534 cm^{-1} is due to the N–O bond stretching of MTZ, confirming the presence of MTZ in the hydrogel and the absence of other peaks of MTZ in the hydrogel shows the presence of interactions between the polymers and the drug (Fig. 1b) [55]. The result indicates the stability of MTZ in the hydrogel. The interaction of MTZ with the hydrogel matrix occurs via this end which reveals MTZ is successfully incorporated into the hydrogel through different physical interactions such as hydrogen bonding and electrostatic attractions.

4.4. X-ray diffraction (XRD)

X-ray diffractograms of pristine CS and SALG are shown in Fig. 6a, of pristine MTZ is shown in Fig. 6b, and of the hydrogels B1–C1

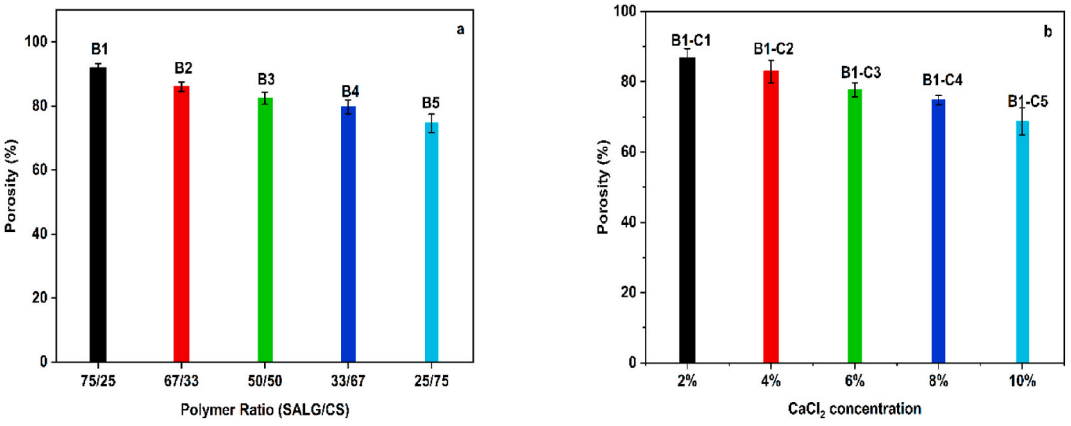

Fig. 4. (a, b). Porosity of hydrogels (a) B1 to B5 (b) B1–C1 to B1–C5.

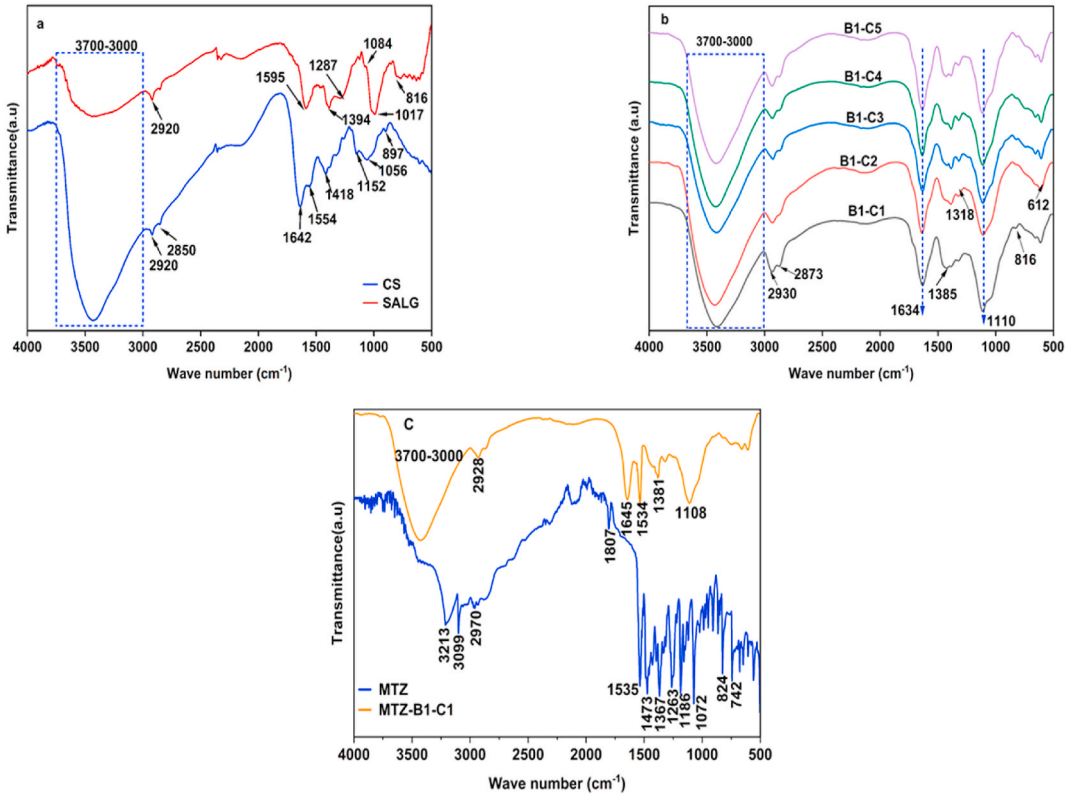

Fig. 5. (a, b, c). FTIR spectra of (a) pristine CS and SALG, (b) hydrogel B1–C1 to B1–C5, and (c) pristine MTZ and hydrogel MTZ- B1–C1.

to B1–C5 and hydrogel MTZ-B1-C1 in Fig. 5c. SALG is normally a crystalline biopolymer. Alginate chains are interconnected via strong hydrogen bonding interactions. SALG shows three diffraction peaks. The first, at 2θ value of 13.6°, is the reflection of the plane (110), originating from the polyguluronate unit; the second, at a 2θ value of 21.5°, is the reflection of the (200) plane from polymannuronate, and the third at 2θ value of 39° is the reflection from the amorphous halo [57]. The diffraction pattern of pristine CS shows the typical crystalline peaks of the polymer with four peaks at 2θ values of 9.6°, 20.2°, 21.3°, and 38.7° corresponding to (020), (200), (201) and (143) diffraction planes, respectively [58]. The first two peaks at 2θ values of 9.6° and 20.2° are slightly lower than the α and β crystal forms of chitosan implying that they are the hydrated form of CS [59]. Metronidazole (Fig. 6b) shows peaks at 2θ values of 12.3°, 13.8°, 24.7° and 29.3. The pattern is similar to those reported in the literature for the drug [60,61]. Due to the crosslinking of CS and SALG the characteristic XRD peaks of each polymer component were disappeared. The XRD spectra of the hydrogels B1–C1 to B1–C5 show a progressive broadening of the peak centered in the range of ca. 17.12° to 17.28° with increasing $CaCl_2$ concentration implying a reduction in crystallinity. During the formation of SALG/CS hydrogels, the hydrogen bonding exist between the $–NH_2$ and –OH groups in CS is broken, leading to amorphous structures of the SALG/CS complex [62].

The decreased crystallinity of the hydrogels also implies that the ionic interaction between SALG and CS led to their excellent compatibility, especially with increasing $CaCl_2$ concentration. The values of 2θ of SALG/CS hydrogels indicate the semi-crystalline nature and the presence of interactions between the polymer chains. The decrease in the intensity of the peaks in the crosslinked hydrogel bead implies the elimination of hydrogen bonding between the $–NH_2$ and –OH groups of chitosan (Kiti & Suwantong, 2020). In the hydrogel MTZ-B1-C1, the sharp diffraction peaks observed in the diffraction pattern of the pristine MTZ are suppressed, probably due to the predominance of the amorphous nature of the hydrogel which shows the molecular miscibility and interaction between the drug and the components. The result confirms that MTZ has been successfully loaded into the hydrogel.

4.5. Thermogravimetric analysis (TGA)

Fig. 7 shows the thermograms of SALG, CS, the hydrogels B1–C1 to B1–C5, and the hydrogel MTZ-B1-C1. The thermogram of SALG shows three steps of mass loss. The first step due to water loss is up to 158 °C with a weight loss of ca. 12%, including free water loss (evaporating between 40 and 60 °C), water interacting with –OH groups (released up to 120 °C), and water bound to carboxyl groups (released up to 160 °C) [63]. The second step, a steep major degradation step, from 205 to 345 °C, with a weight loss of ca. 38% is due to the complexity of the degradation of the alginate backbone (glucosidic bonds) [63] leading to the formation of water, CH_4 and release of CO_2 by the degradation of the carboxylate group and also the formation of Na_2CO_3. The third weight loss of ca. 26% between 350 °C to 700 °C is due to the degradation of the fragments and monomeric units of the alginate into Na_2CO_3, and degradation of

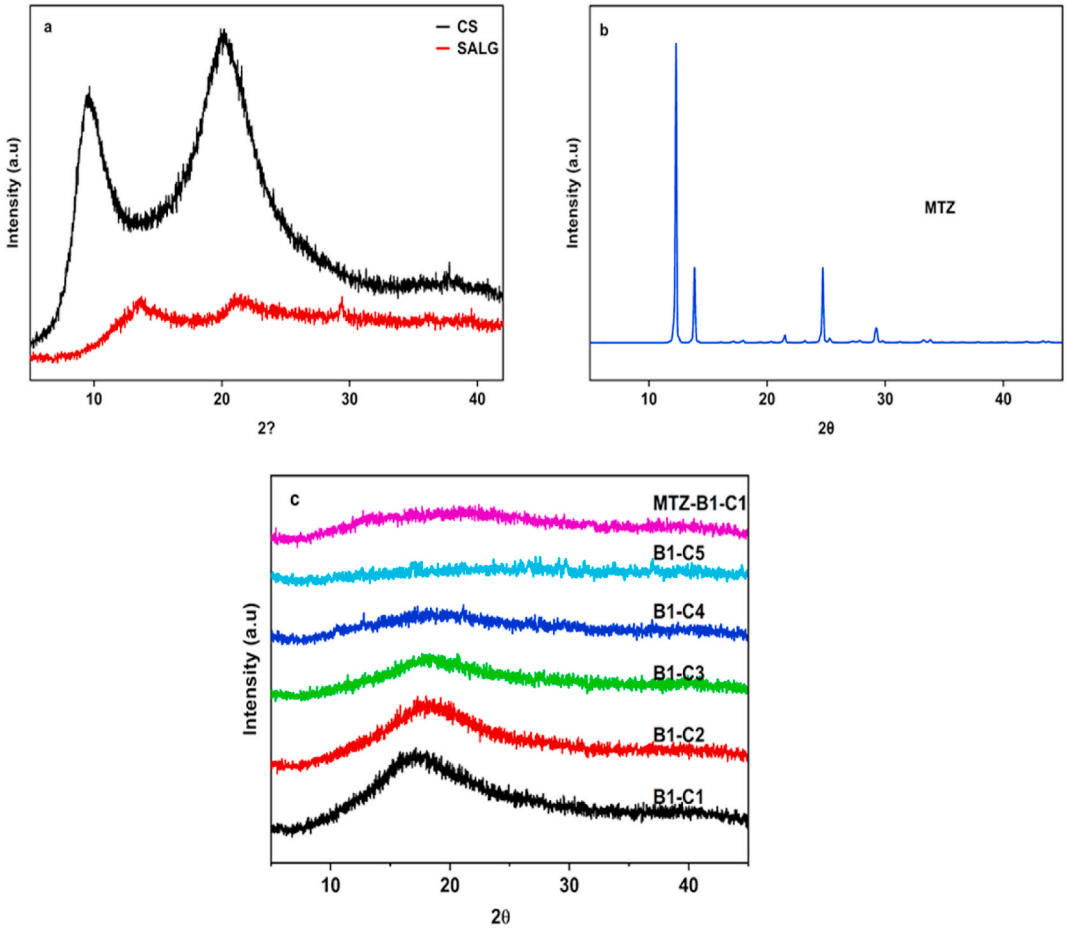

Fig. 6. (a, b, c). XRD diffractograms of (a) pristine CS and SALG, (b) pristine MTZ and (c) hydrogels B1–C1to B1–C5 and MTZ-B1-C1.

Na_2CO_3 to NaO and CO_2 [64].

There are three separate weight loss steps in CS. The first weight loss step of ca. 7% up to 115 °C is due to the loss of easily removed free water, which does not interact via secondary interactions. A gradual slope follows this till 214 °C with a further weight loss of ca. 8% due to loss of bound water contained in the hydrophilic functional groups. The second mass loss step of ca. 32% in the range of 214 °C to 367 °C is because of the partial degradation of the polymer with crosslinking reactions occurring resulting from the

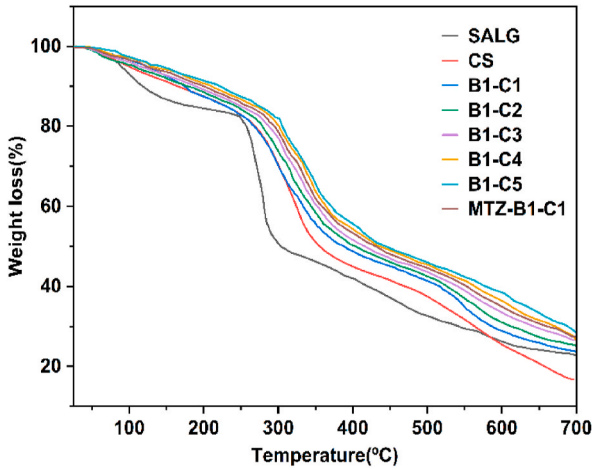

Fig. 7. TGA thermograms of pristine SALG and CS, hydrogels B1–C1 to B1–C5, and MTZ-B1-C1.

destruction of –NH_2 groups [65,66]. The third weight loss step at higher temperatures, ca. 435 °C to 700 °C is because of the complete degradation of the networked material formed by thermal crosslinking reactions that occur in the second step with a final remaining mass (ash) of ca. 17%. The thermal degradation of CS is amalgamated with with an intricate process in which the polysaccharide rings are dried, and the acetylated and deacetylated CS units are depolymerized and decomposed.

The thermograms of the hydrogels B1–C1 to B1–C5 and MTZ-B1-C1 show that mass loss occurs in three steps. Overall, all the double crosslinked hydrogels show lower free water weight lost at the initial step compared to SALG and CS and required higher temperatures up to ca. 175 ºC to release the absorbed water due to its stronger immobilization between the crosslinked CS chains. A reduced interactions between water molecules with anionic SALG and cationic CS ends resulted in a lower swelling capacity of hydrogel microbeads [67]. The most significant changes are obtained beyond 220 °C. The second step, the foremost mass loss step, between ca. 220 °C to ca. 380 °C, involves the release of water bound to the COO- of SALG and –NH_3^+ ends of CS, not completely eliminate in the first step of water loss, the degradation of the –COOH groups and deacetylation and partial depolymerization of CS. The third mass loss between ca. 465 °C to 700 °C is associated with complete degradation and formation of ash. The thermal stability of the hydrogels is increased due to the crosslinking of the polymers and the complexation of SALG with CS.

4.6. Gel fraction

The gel contents of the hydrogels B1 to B5 and hydrogels B1–C1 to B1–C5, respectively are shown in Fig. 8a, b. Hydrogel B1 displays the lowest gel content of ca. 77%, and hydrogel B5 shows the highest gel content of ca. 90% (Fig. 8a). This indicates that the gel content increases with crosslinked CS content, which is attributed to an increase in the formation of CS and SALG networks, resulting in denser interpenetrated networks. The stronger and more rigid the hydrogel structures become, the less becomes the ingress rate of the dissolution medium into the matrices.

The gel content of the select hydrogel B1 is shown in Fig. 8b as a function of $CaCl_2$ concentration. As the cationic crosslinking agent amount increases, the gel content increases, inferring that it can crosslink more efficiently with SALG because a greater quantity of Ca^{2+} ions is available to bind. This results in decreased network space. Furthermore, the number of –COO– groups decreases as more and more Ca^{2+} cations combine with the –COOH groups of SALG. The overall result is a weakening of the electrostatic repulsion between the –COO– groups and the hydrogel matrices are transformed into stronger and rigid structures, which do not allow the ingress of the dissolution media into the matrices at higher rates [27,68].

4.7. Biodegradation

The in vitro degradation of the hydrogel microbeads B1–C1 to B1–C5 and MTZ-B1-C1 immersed in SCF (pH 7.4) at 37.2 °C for 30 days are shown in Fig. 9. From the figure it is observed that the hydrogel beads show a similar degradation behavior, the only difference being a reduction in weight loss with increasing $CaCl_2$ content. Hydrogel beads B1–C1 and B1–C2 degraded at a relatively higher rate and reached weight loss of 39.58 5% and 35.38% respectively between day 1 and day 7.

While hydrogel beads B1–C3, B1–C4, and B1–C5 showed weight loss of 24.5%, 14.8%, and 11.5% within the first 7 days. The weight loss behavior also shows that irrespective of the $CaCl_2$ content, the rate of degradation between day 7 and day 30 is relatively slower. The decrease in weight loss with increasing $CaCl_2$ content is attributed to an increase in inter-chain SALG polymer networking with Ca^{2+} (“egg-box” dimer) leading to the formation of more compact and dense structures [69]. The effect of CS on degradation is consistent with the fact that CS with a higher degree of deacetylation has better biological properties than CS with low degrees of deacetylation [70].

The degradation of the drug loaded hydrogel (MTZ-B1-C1) is observed to be lower than that of the corresponding unloaded hydrogel B1–C1 with a weight loss of about 60% in 30 days. This might be associated with the presence of improved interactions among the polymer matrixes and the drug resulted in the formation of a more stable crosslinked structure [71]. Generally, the degradation rate of the CS/SALG hydrogel beads in this work is low due to the double crosslinking of SALG and CS using

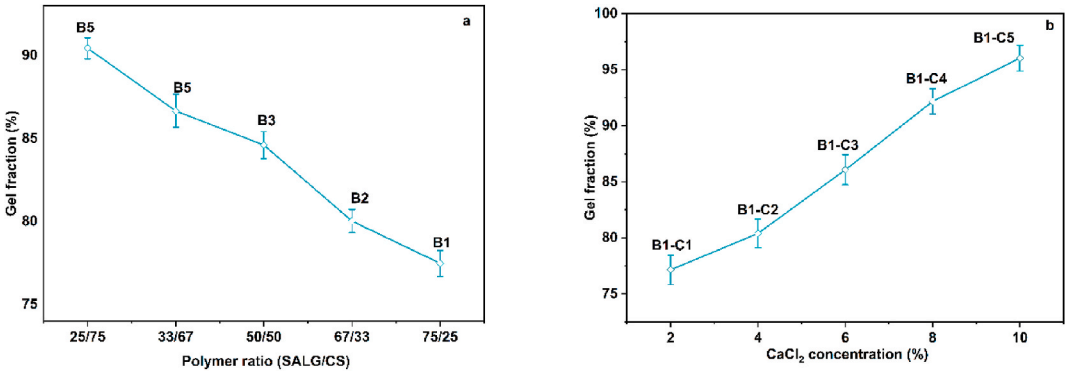

Fig. 8. (a, b). Gel fraction of (a) hydrogels B1 to B5 and (b) hydrogel B1 as a function of CaCl2 concentration.

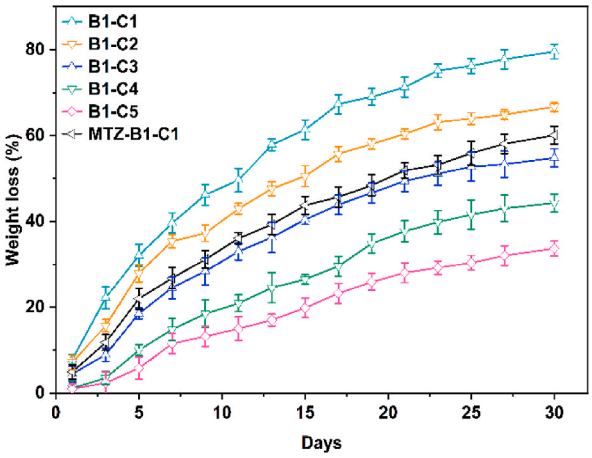

Fig. 9. In vitro degradation of hydrogels B1–C1 to B1–C5 in SCF (pH 7.4) at 37 °C for 30 days.

glutaraldehyde which helps the hydrogels to withstand the effects of gastric medium (acidic), small intestinal and colon physiological fluids for the controlled and sustained release of MTZ. The biodegradation behavior of the hydrogel beads in this study is consistent with the results of previous studies [70,71].

4.8. Field emission scanning electron microscopy (FESEM)

Fig. 10a-f shows the SEM micrographs of hydrogels B1–C1 to B1–C5 and MTZ-B1-C1. All hydrogels show a porous surface structure but with distinct differences in pore size, pore uniformity, and the thickness of the polymer wall surrounding the pores as a function of $CaCl_2$ content.

The structures of hydrogels B1–C1 to B1–C5 (Fig. 10a–e) show interconnected porous, fibrous, and rough 3D network topology.

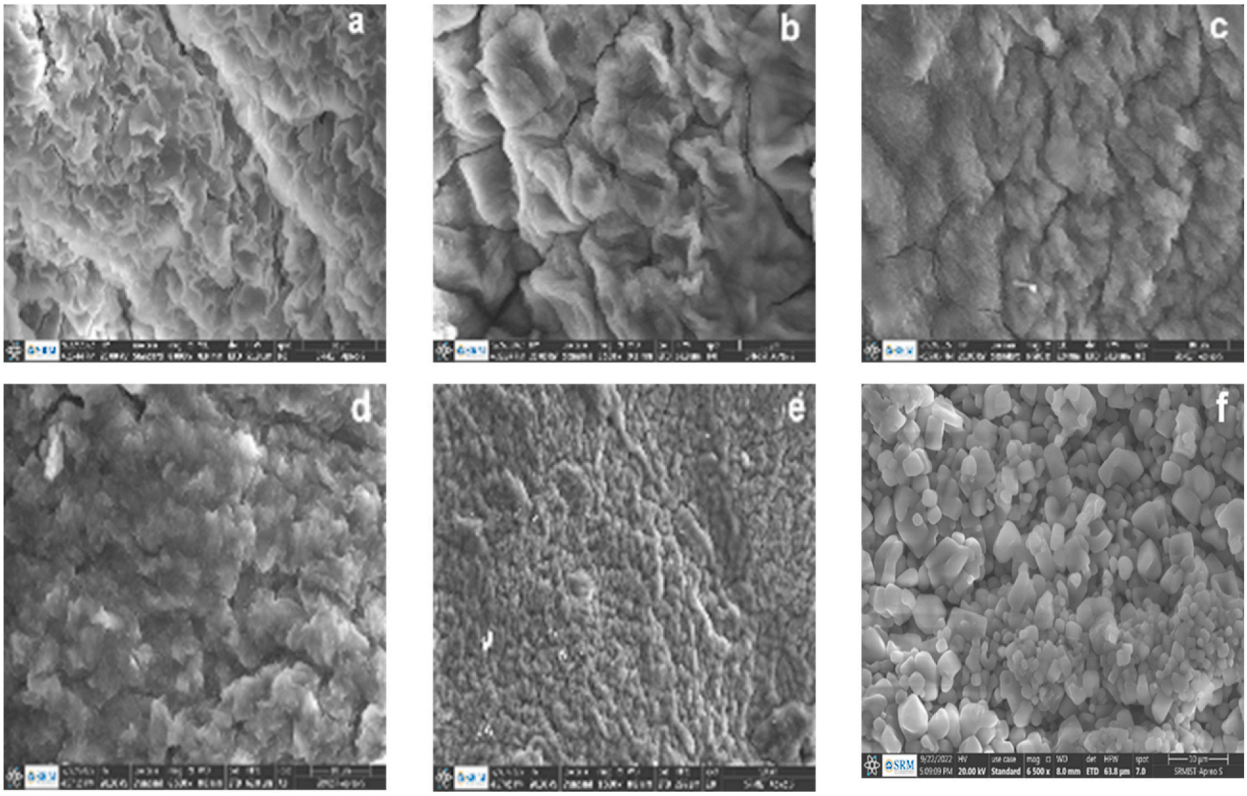

Fig. 10. (a–f). FESEM micrographs of (a–e) hydrogels B1–C1 to B1–C5 and (f) hydrogel MTZ- B1–C1.

These surface features, pore size, and uniformity of pores reduce with increasing $CaCl_2$ content, inferring densification of the matrices. This morphology and reduced pore size infer a higher degree of matrix densification with a further increase in $CaCl_2$ concentration. These features of the hydrogels are consistent with their corresponding swelling ability and pH responsive behaviour. For example, the highly densified structures and tiny or closed pores of the hydrogels B1–C4 and B1–C5 lead to reduced ability of the simulated physiological fluids to ingress within the hydrogels showing that the swelling degree and pH sensitivity of the hydrogels is gradually decreased when the concentration of $CaCl_2$ increased from 2 to 10%.

The morphology of hydrogel MTZ-B1-C1 (Fig. 10f) shows the surface texture of relatively highly granulated but smooth surfaces and smaller inner pores confirming the successful incorporation and miscibility of MTZ particles into the hydrogel. Therefore, the micrograph of MTZ-B1-C1 shows that MTZ particles are present in the pores and on the surface of the hydrogel. Hence, the pore structure of the hydrogel B1–C1 is considered a potent candidate for the controlled release of MTZ.

4.9. In vitro MTZ release

The cumulative release of MTZ from MTZ-B1-C1 in SGF (pH 1.2), SIF (pH 6.8), and SCF (pH 7.4) at 37 °C is shown in Fig. 11. The drug release after the first 1 h is ca. 9%, 13%, and 17% in SGF, SIF, and SCF, respectively. After that, the release follows a monotonic increasing release pattern with time, irrespective of the simulated physiological fluid pH. At 24 h, the cumulative drug release is ca. 62%, 73%, and 81.74% in SGF, SIF, and SCF, respectively, showing the influence of the medium pH since both SALG and CS are pH-sensitive polysaccharides based on their swelling properties.

In SGF, the low MTZ release can be explained by the formation of the insoluble form of alginic acid due to the protonation of SALG. In SGF (pH 1.2 < pKa 3.4 of SALG), SALG chains protonate to produce –COOH groups. Hydrogen bonds are formed between the –COOH and –OH groups, creating an insoluble SALG barrier on the surface of the hydrogel, which protects the structure from fluid ingress and hinders swelling [72]. At the same time, CS inhibits drug release due to the strong interaction of its positively charged groups with SALG, thus reducing hydrogel swelling and, therefore, drug release. As the pH increases to 6.8 and 7.4, the increasing deprotonation of SALG with pH causes the disintegration of the hydrogel via stretching of the SALG chains releasing its free surface because of the electrostatic repulsion force between $–COO^-$ anions. This relaxation of the polymer chains increases fluid ingress into the hydrogel structure and, thus, drug release.

4.10. Drug release kinetics

The cumulative percentage MTZ release data were applied to different release kinetic models such Higuchi, Korsmeyer–Peppas, first-order, and zero-order to estabilish the release mechanism of MTZ from the optimum SALG/CS hydrogel bead (B1–C1). The corresponding results of each linear fitted model of the release rate of MTZ in SGF (pH 1.2), SIF (pH 7.4), and SCF (pH 7.4) as a function of time are presented in Table 3. The model that best fits MTZ release pattern was selected based on the highest coefficient of correlation (R^2).

From the release kinetics of MTZ in SGF (pH 1.2), SIF (pH 6.8), and SCF (pH 7.4), it is seen that the Korsmeyer–Peppas model shows the highest R^2 value of 0.9781, 0.9739 and 0.9458 respectively. These results show the Korsmeyer–Peppas model is the best fit for the release of MTZ in all simulated media. Furthermore, the calculated exponents n determined for the controlled release of MTZ in SGF, SIF, and SCF from the Korsmeyer-Peppas kinetic model is 0.653, 0.5977, and 0.5645 respectively which suggests the release of MTZ from the hydrogel bead B1–C1 follows anomalous mechanism or combinations of diffusion and swelling controlled time-dependent non-Fickian mechanism (0.43 < n < 0.85) [73].

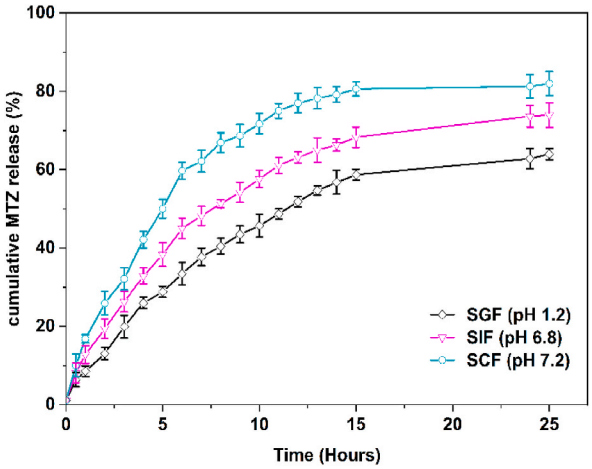

Fig. 11. Cumulative MTZ release from the hydrogel MTZ-B1-C1 in SGF, SIF and SGF at 37.2 °C.

4.11. Antibacterial test

The synergetic antibacterial effect of the polymer matrix (chitosan) and metronidazole was tested against *Staphylococcus aureus and Escherichia coli* which were selected based on previous studies [39,74]. The zone inhibition diameter of the test samples (mm) against *Staphylococcus aureus* (ATCC25923) and *Escherichia coli* (ATCC25922*)* is shown in Table 4.

Fig. 12 (a, b) shows the photographs of the inhibition zones of the pristine MTZ (positive control), B1–C1 (negative control), and MTZ-B1-C1 with significant inhibitory growth against the bacteria species. The hydrogel MTZ-B1-C1 inhibited the *Staphylococcus aureus* and *Escherichia coli* bacteria with zones of inhibition ranging from 18.35 $\pm$ 0.5 mm and 17.4 $\pm$ 0.2 respectively (Table 4). This shows that the drug loaded hydrogel is significantly inhibited the growth of the bacteria species. The lower inhibition zone of the unloaded hydrogel relative to that of the drug loaded hydrogel is may be due to the antibacterial nature of CS [75]. CS binds to the bacterial DNA via its cationic amine groups inhibiting protein and mRNA synthesis of the bacterial species [76]. Its antibacterial activity is directly proportional to its degree of deacetylation (in this study, CS is $\geq$ 75% deacetylated), which in turn is related to the number of the protonated amine groups. The significantly lower zones of inhibition observed around pure MTZ (PC) shows that the bacteria species are less sensitive to the drug. The significant antibacterial activity of the hydrogel MTZ-B1-C1 is possibly because of the synergistic activity of CS and MTZ released from the hydrogel matrix on swelling [77]. Metronidazole is nitroimidazole drug act by interacting with DNA of bacteria forming nitroso radicals and hydroxyl amine derivatives which causes the loss of helical structure of DNA of the microbial cells, and therefore causes cell death of the susceptible organisms [78]. From these results, the MTZ loaded SALG/CS hydrogel possibly will have clinical inferences which requires further studied for use in CDDSs.

5. Conclusion

Double-crosslinked SALG/CS hydrogels with different ratios of the polymers crosslinked by $CaCl_2$ and glutaraldehyde were prepared. All hydrogel compositions displayed pH sensitivity to swelling in physiological fluids. The increase in CS amount caused a decrease in porosity and an increase in gel fraction due to crosslinking by glutaraldehyde. Based on the lowest swelling ratio at pH 1.2 and the highest swelling ratio at pH 7.4, a hydrogel composition of SALG/CS of weight ratio of 75/25 was chosen for optimization by varying the $CaCl_2$ concentration from 2 to 10% for the loading of MTZ and its controlled release at pH 1.2, 6.8 and 7.4. The hydrogel composition crosslinked with 2% $CaCl_2$ was deemed to be optimal in comparison to other concentrations for MTZ loading as it displayed the highest percent porosity, lowest gel fraction, well-distributed pores, and a less dense structure, low matrix crystallinity, good thermal stability, and the highest percent in vitro biodegradability. This hydrogel loaded with MTZ showed a surface texture of relatively highly granulated but smooth surfaces and smaller inner pores confirming the successful incorporation and miscibility of MTZ particles into the hydrogel. The observed morphology of MTZ-B1-C1 is associated with the enhanced interactions between SALG, CS, and MTZ, forming a more stable crosslinked structure and a good cumulative drug release profile that followed the diffusion and swelling-controlled non-Fickian mechanism. The significant antibacterial activity, because of the synergistic activity of CS and the MTZ released from the matrix on swelling, makes this hydrogel a good suggestion to be applied in antimicrobial applications such as CDDS and wound dressing.

Funding

None.

Author contribution statement

Zerihun Feyissa: Conceived and designed the experiments; Performed the experiments; Analyzed and interpreted data; Wrote the paper.

Gemechu Deressa Edossa: Contributed reagents, materials; Analyzed and interpreted data; Wrote the paper.

Neeraj Kumar Gupta: Conceived and designed the experiments; Analyzed and interpreted data; Wrote the paper.

Defaru Negera: Contributed reagents, materials, analysis tools or data.

Data availability statement

Data will be made available on request.

Additional information

No additional information is available for this paper.

Declaration of competing interest

The authors declare that they have no known competing financial interests or personal relationships that could have appeared to influence the work reported in this paper.

Table 3
Drug release kinetics for MTZ release from the hydrogel B1–C1.

pH	Zero-Order Model		First Order Model		Higuchi model		Korsmeyer–Peppas	
	K_0	R^2	K_1	R^2	K_H	R^2	n	R^2
1.2	1.2036	0.8424	0.0789929	0.6483	7.5386	0.9609	0.652	0.9781
6.8	1.3206	0.8	0.0704718	0.6117	8.4153	0.9444	0.5977	0.9739
7.4	1.3949	0.6883	0.0633325	0.5402	9.2154	0.8735	0.5645	0.9458

Table 4
The cumulative zone of inhibition of MTZ-B1-C1.

No	Bacterial strain	Zone inhibition Diameter of Test samples (mm)		
		Negative control (NC)	Positive control (PC)	MTZ loaded Hydrogel
1	*Staphylococcus aureus(ATCC25923)*	8.3 ± 0.5	10.4 ± 0.7	18.35 ± 0.5
2	*Escherichia coli (ATCC25922)*	6.3 ± 0.3	10.1 ± 0.5	17.4 ± 0.2

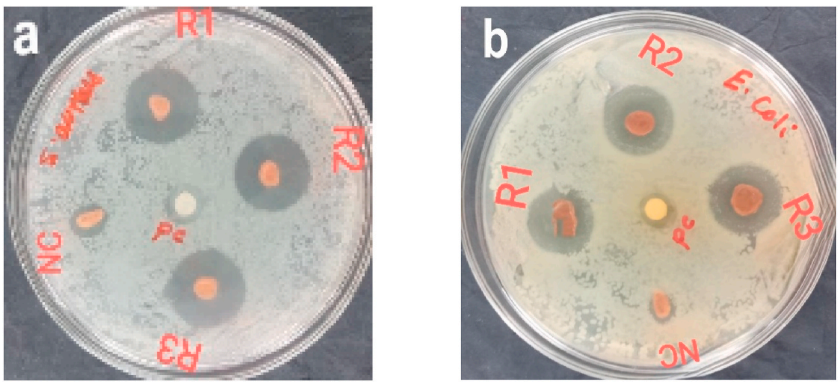

Fig. 12. (a, b). Disc diffusion assays showing zone of inhibition exhibited by unloaded B1–C1 (NC), MTZ-B1-C1 and pure metronidazole (pc) against a) *Staphylococcus aureus* b) *Escherichia coli.*

Acknowledgements

The authors would like to thank Adama Science and Technology University, Adama, Ethiopia, Ethiopian Ministry of Education, Ethiopia and SRM Institute of Science and Technology, Kattan kulathur, India, extending facilities to undertake experiments and characterization for this work.

References

[1] H.M. Jeong, K.Y. Weon, B.S. Shin, S. Shin, 3D-printed gastroretentive sustained release drug delivery system by applying design of experiment approach, Molecules 25 (2020), https://doi.org/10.3390/molecules25102330.
[2] I.M. Oliveira, C. Gonçalves, M.E. Shin, S. Lee, R.L. Reis, G. Khang, Enzymatically crosslinked tyramine-gellan gum hydrogels as drug delivery system for rheumatoid arthritis treatment, Drug Deliv. Transl. Res. 11 (2021) 1288–1300, https://doi.org/10.1007/s13346-020-00855-9.
[3] A. Vashist, A. Vashist, Y.K. Gupta, S. Ahmad, Recent advances in hydrogel based drug delivery systems for the human body (2014) 147–166, https://doi.org/10.1039/c3tb21016b.
[4] K. Dutta, R. Das, J. Ling, R.M. Monibas, E. Carballo-Jane, A. Kekec, D.D. Feng, S. Lin, J. Mu, R. Saklatvala, S. Thayumanavan, Y. Liang, In situ forming injectable thermoresponsive hydrogels for controlled delivery of biomacromolecules, ACS Omega 5 (2020) 17531–17542, https://doi.org/10.1021/acsomega.0c02009.
[5] S. Nawaz, S. Khan, U. Farooq, M.S. Haider, N.M. Ranjha, A. Rasul, A. Nawaz, N. Arshad, R. Hameed, Biocompatible hydrogels for the controlled delivery of anti-hypertensive agent: development, characterization and in vitro evaluation, Des. Monomers Polym. 21 (2018) 18–32, https://doi.org/10.1080/15685551.2018.1445416.
[6] J.S. Yoneda, D.R. de Araujo, F. Sella, G.R. Liguori, T.T.A. Liguori, L.F.P. Moreira, F. Spinozzi, P. Mariani, R. Itri, Self-assembled guanosine-hydrogels for drug-delivery application: structural and mechanical characterization, methylene blue loading and controlled release, Mater. Sci. Eng. C 121 (2021), 111834, https://doi.org/10.1016/j.msec.2020.111834.
[7] R. Narayanaswamy, V.P. Torchilin, Hydrogels and their applications in targeted drug delivery, Molecules 24 (2019), https://doi.org/10.3390/molecules24030603.
[8] M.J. Webber, E.T. Pashuck, (Macro)molecular self-assembly for hydrogel drug delivery, Adv. Drug Deliv. Rev. 172 (2021) 275–295, https://doi.org/10.1016/j.addr.2021.01.006.
[9] W.E. Hennink, C.F. van Nostrum, Novel crosslinking methods to design hydrogels, Adv. Drug Deliv. Rev. 64 (2012) 223–236, https://doi.org/10.1016/j.addr.2012.09.009.
[10] J. Maitra, V.K. Shukla, Cross-linking in hydrogels - a review, Am. J. Polym. Sci. 4 (2014) 25–31, https://doi.org/10.5923/j.ajps.20140402.01.

[11] D. Aycan, N.A. Yayla, Y.A. Aydin, Chitosan polyvinyl alcohol blend films for ibuprofen encapsulation: fabrication, characterization and kinetics, Polym. Degrad. Stabil. 181 (2020), 109346, https://doi.org/10.1016/j.polymdegradstab.2020.109346.

[12] I. Călina, M. Demeter, A. Scărişoreanu, V. Sătulu, B. Mitu, One step e-beam radiation cross-linking of quaternary hydrogels dressings based on chitosan-poly (Vinyl-pyrrolidone)-poly(ethylene glycol)-poly(acrylic acid), Int. J. Mol. Sci. 21 (2020) 1–24, https://doi.org/10.3390/ijms21239236.

[13] R.H. Sizílio, J.G. Galvão, G.G.G. Trindade, L.T.S. Pina, L.N. Andrade, J.K.M.C. Gonsalves, Chitosan/pvp-based mucoadhesive membranes as a promising delivery system of betamethasone-17-valerate for aphthous stomatitis, Carbohydr. Polym. 190 (2018) 339–345, https://doi.org/10.1016/j.carbpol.2018.02.079.

[14] I.A. Duceac, L. Verestiuc, C.D. Dimitriu, V. Maier, S. Coseri, Design and preparation of new multifunctional hydrogels based on chitosan/acrylic polymers for drug delivery and wound dressing applications, Polym. (Basel) 12 (2020) 1–20, https://doi.org/10.3390/polym12071473.

[15] J. Pan, Y. Li, K. Chen, Y. Zhang, H. Zhang, Enhanced physical and antimicrobial properties of alginate/chitosan composite aerogels based on electrostatic interactions and noncovalent crosslinking, Carbohydr. Polym. 266 (2021), 118102, https://doi.org/10.1016/j.carbpol.2021.118102.

[16] A.K. Nayak, M.S. Hasnain, Advanced Biopolymeric Systems for Drug Delivery, Springer Nature, 2020, 9783030469221.

[17] E.S. Costa-Júnior, E.F. Barbosa-Stancioli, A.A.P. Mansur, W.L. Vasconcelos, H.S. Mansur, Preparation and characterization of chitosan/poly(vinyl alcohol) chemically crosslinked blends for biomedical applications, Carbohydr. Polym. 76 (2009) 472–481, https://doi.org/10.1016/j.carbpol.2008.11.015.

[18] R.H. Sizílio, J.G. Galvão, G.G.G. Trindade, L.T.S. Pina, L.N. Andrade, J.K.M.C. Gonsalves, A.A.M. Lira, M.V. Chaud, T.F.R. Alves, M.L.P.M. Arguelho, R.S. Nunes, Chitosan/pvp-based mucoadhesive membranes as a promising delivery system of betamethasone-17-valerate for aphthous stomatitis, Carbohydr. Polym. 190 (2018) 339–345, https://doi.org/10.1016/j.carbpol.2018.02.079.

[19] Y.C. Danarto, Budhijanto Rochmadi, Microencapsulation of riboflavin (vitamin B2) using alginate and chitosan : effect of alginate and chitosan concentration upon encapsulation efficiency, IOP Conf. Ser. Mater. Sci. Eng. 858 (2020), https://doi.org/10.1088/1757-899X/858/1/012030.

[20] J. Potaś, E. Szymańska, K. Winnicka, Challenges in developing of chitosan – based polyelectrolyte complexes as a platform for mucosal and skin drug delivery, Eur. Polym. J. 140 (2020), 110020, https://doi.org/10.1016/j.eurpolymj.2020.110020.

[21] A. Dodero, L. Pianella, S. Vicini, M. Alloisio, M. Ottonelli, M. Castellano, Alginate-based hydrogels prepared via ionic gelation : an experimental design approach to predict the crosslinking degree, Eur. Polym. J. 118 (2019) 586–594, https://doi.org/10.1016/j.eurpolymj.2019.06.028.

[22] S. Masoomi Dezfooli, C. Bonnot, N. Gutierrez-Maddox, A.C. Alfaro, A. Seyfoddin, Chitosan coated alginate beads as probiotic delivery system for New Zealand black footed abalone (Haliotis iris), J. Appl. Polym. Sci. 139 (2022) 1–15, https://doi.org/10.1002/app.52626.

[23] T. Wu, S. Yu, D. Lin, Z. Wu, J. Xu, J. Zhang, Z. Ding, Y. Miao, T. Liu, T. Chen, X. Cai, Preparation, characterization, and release behavior of doxorubicin hydrochloride from dual cross-linked chitosan/alginate hydrogel beads, ACS Appl. Bio Mater. 3 (2020) 3057–3065, https://doi.org/10.1021/acsabm.9b01119.

[24] M. Matyash, F. Despang, C. Ikonomidou, M. Gelinsky, Swelling and mechanical properties of alginate hydrogels with respect to promotion of neural growth, Tissue Eng. - Part C Methods. 20 (2014) 401–411, https://doi.org/10.1089/ten.tec.2013.0252.

[25] N.K. Muhammad Firdaus Kumar, C.C. Meng, N.H.A. Manas, R.A. Ahmad, S.F.Z. Mohd Fuzi, R.A. Rahman, R. Md Illias, Immobilization of maltogenic amylase in alginate-chitosan beads for improved enzyme retention and stability, Malaysian J. Fundam. Appl. Sci. 18 (2022) 43–51, https://doi.org/10.11113/MJFAS.V18N1.2381.

[26] A. Banerjee, S. Ganguly, Alginate–chitosan composite hydrogel film with macrovoids in the inner layer for biomedical applications, J. Appl. Polym. Sci. 136 (2019) 30–33, https://doi.org/10.1002/app.47599.

[27] G. Rassu, A. Salis, E. Piera, P. Giunchedi, M. Roldo, E. Gavini, Composite chitosan/alginate hydrogel for controlled release of deferoxamine : a system to potentially treat iron dysregulation diseases, Carbohydr. Polym. 136 (2016) 1338–1347, https://doi.org/10.1016/j.carbpol.2015.10.048.

[28] S. Bensouiki, F. Belaib, M. Sindt, P. Magri, S. Rup, J. Chawki, Evaluation of anti - inflammatory activity and in vitro drug release of ibuprofen - loaded nanoparticles based on sodium alginate and chitosan, Arab. J. Sci. Eng. (2020), https://doi.org/10.1007/s13369-020-04720-2.

[29] X. Tao, X.J. Sun, J. Su, J.F. Chen, W. Roa, Natural microshells of alginate-chitosan: unexpected stability and permeability, Polymer (Guildf). 47 (2006) 6167–6171, https://doi.org/10.1016/j.polymer.2006.06.038.

[30] S. Tang, J. Yang, L. Lin, K. Peng, Y. Chen, S. Jin, W. Yao, Construction of physically crosslinked chitosan/sodium alginate/calcium ion double-network hydrogel and its application to heavy metal ions removal, Chem. Eng. J. 393 (2020), 124728, https://doi.org/10.1016/j.cej.2020.124728.

[31] K.A. Wilk, S. Balicki, P. Warszy, Insight into multilayered alginate/chitosan microparticles for oral administration of large cranberry fruit extract (2021) 160, https://doi.org/10.1016/j.eurpolymj.2021.110776.

[32] M.M. Rahman, F.I. Jahan, N.F. Fahim, N. Paul, N. Jahan, M. Harun-Or-rashid, S.Z. Tanny, In vitro comparative quality evaluation of leading brands of metronidazole tablets available in Bangladesh, Pharmacologyonline 2 (2020) 63–72. http://pharmacologyonline.silae.it/. accessed on 1, Jun3, 2023.

[33] M. Okuda, Y. Lin, C. Wang, T. Kakiuchi, S. Kikuchi, Metronidazole for Helicobacter pylori eradication therapy among children and adolescents in Japan: overcoming controversies and concerns, Helicobacter 24 (2019) 1–6, https://doi.org/10.1111/hel.12575.

[34] M.K. Katual, Formulation, optimization and in-vitro evaluation of metronidazole 500Mg floating tablets for the treatment of Helicobacter pylori induced gastric inflammatory disorder, World J. Pharm. Res. (2017) 809–835, https://doi.org/10.20959/wjpr20174-8253.

[35] M.R.C. Marques, R. Loebenberg, M. Almukainzi, Simulated biological fluids with possible application in dissolution testing, Dissolution Technol. 18 (2011) 15–28, https://doi.org/10.14227/DT180311P15.

[36] K. Kiti, O. Suwantong, Bilayer wound dressing based on sodium alginate incorporated with curcumin-β-cyclodextrin inclusion complex/chitosan hydrogel, Int. J. Biol. Macromol. 164 (2020) 4113–4124, https://doi.org/10.1016/j.ijbiomac.2020.09.013.

[37] S. Saeedi Garakani, S.M. Davachi, Z. Bagher, A. Heraji Esfahani, N. Jenabi, Z. Atoufi, M. Khanmohammadi, A. Abbaspourrad, H. Rashedi, M. Jalessi, Fabrication of chitosan/polyvinylpyrrolidone hydrogel scaffolds containing PLGA microparticles loaded with dexamethasone for biomedical applications, Int. J. Biol. Macromol. 164 (2020) 356–370, https://doi.org/10.1016/j.ijbiomac.2020.07.138.

[38] F.A. Ngwabebhoh, O. Zandraa, R. Patwa, N. Saha, Z. Capáková, P. Saha, Self-crosslinked chitosan/dialdehyde xanthan gum blended hypromellose hydrogel for the controlled delivery of ampicillin, minocycline and rifampicin, Int. J. Biol. Macromol. 167 (2021) 1468–1478, https://doi.org/10.1016/j.ijbiomac.2020.11.100.

[39] P.P. Rade, P.S. Giram, A.A. Shitole, N. Sharma, B. Garnaik, Physicochemical and in vitro antibacterial evaluation of metronidazole loaded eudragit S-100 nanofibrous mats for the intestinal drug delivery, Adv. Fiber Mater. 4 (2022) 76–88, https://doi.org/10.1007/s42765-021-00090-y.

[40] D.K. Khajuria, R. Vasireddi, M.K. Priydarshi, D.R. Mahapatra, Ionic diffusion and drug release behavior of core-shell-functionalized alginate-chitosan-based hydrogel, ACS Omega 5 (2020) 758–765, https://doi.org/10.1021/acsomega.9b03464.

[41] K. Baysal, A.Z. Aroguz, Z. Adiguzel, B.M. Baysal, Chitosan/alginate crosslinked hydrogels: preparation, characterization and application for cell growth purposes, Int. J. Biol. Macromol. 59 (2013) 342–348, https://doi.org/10.1016/j.ijbiomac.2013.04.073.

[42] J. Adhikari, M.S. Perwez, A. Das, P. Saha, Development of hydroxyapatite reinforced alginate–chitosan based printable biomaterial-ink, Nano-Structures and Nano-Objects 25 (2021), 100630, https://doi.org/10.1016/j.nanoso.2020.100630.

[43] G. Lawrie, I. Keen, B. Drew, A. Chandler-Temple, L. Rintoul, P. Fredericks, L. Grøndahl, Interactions between alginate and chitosan biopolymers characterized using FTIR and XPS, Biomacromolecules 8 (2007) 2533–2541, https://doi.org/10.1021/bm070014y.

[44] H. Li, X. Wang, Z. Wang, K.Y. Lam, Multiphysics modelling of volume phase transition of ionic hydrogels responsive to thermal stimulus, Macromol. Biosci. 5 (2005) 904–914, https://doi.org/10.1002/mabi.200500082.

[45] M.R. Guilherme, M.R. De Moura, E. Radovanovic, G. Geuskens, A.F. Rubira, E.C. Muniz, Novel thermo-responsive membranes composed of interpenetrated polymer networks of alginate-Ca2+ and poly(N-isopropylacrylamide), Polymer (Guildf) 46 (2005) 2668–2674, https://doi.org/10.1016/j.polymer.2005.01.082.

[46] S.A.P. Siboro, D.S.B. Anugrah, K. Ramesh, S.H. Park, H.R. Kim, K.T. Lim, Tunable porosity of covalently crosslinked alginate-based hydrogels and its significance in drug release behavior, Carbohydr, Polym 260 (2021), 117779, https://doi.org/10.1016/j.carbpol.2021.117779.

[47] A. Radhakrishnan, G. Mariya, J. Muraleedhara, PEG-penetrated chitosan – alginate co-polysaccharide-based partially and fully cross-linked hydrogels as ECM mimic for tissue engineering applications, Prog. Biomater. 4 (2015) 101–112, https://doi.org/10.1007/s40204-015-0041-3.

[48] J. Nastaj, A. Przewłocka, M. Rajkowska-Myśliwiec, Biosorption of Ni(II), Pb(II) and Zn(II) on calcium alginate beads: equilibrium, kinetic and mechanism studies, Polish J. Chem. Technol. 18 (2016) 81–87, https://doi.org/10.1515/pjct-2016-0052.
[49] T. Peng, K. De Yao, C. Yuan, M.F.A. Goosen, Structural changes of pH-sensitive chitosan/polyether hydrogels in different pH solution, J. Polym. Sci. Part A Polym. Chem. 32 (1994) 591–596, https://doi.org/10.1002/pola.1994.080320322.
[50] A. Rahma, M.M. Munir, Khairurrijal, A. Prasetyo, V. Suendo, H. Rachmawati, Intermolecular interactions and the release pattern of electrospun curcumin-polyvinyl(pyrrolidone) fiber, Biol. Pharm. Bull. 39 (2016) 163–173, https://doi.org/10.1248/bpb.b15-00391.
[51] J. Han, Z. Zhou, R. Yin, D. Yang, J. Nie, Alginate-chitosan/hydroxyapatite polyelectrolyte complex porous scaffolds: preparation and characterization, Int. J. Biol. Macromol. 46 (2010) 199–205, https://doi.org/10.1016/j.ijbiomac.2009.11.004.
[52] S. Bashir, Y.Y. Teo, S. Ramesh, K. Ramesh, Synthesis, characterization, properties of N-succinyl chitosan-g-poly (methacrylic acid) hydrogels and in vitro release of theophylline, Polymer (Guildf) 92 (2016) 36–49, https://doi.org/10.1016/j.polymer.2016.03.045.
[53] B.K. Heragh, S. Javanshir, G.R. Mahdavinia, M.R. Naimi-Jamal, Development of pH-sensitive biomaterial-based nanocomposite for highly controlled drug release, Results Mater 16 (2022), 100324, https://doi.org/10.1016/j.rinma.2022.100324.
[54] A.V. Myhal, O.S. Golovchenko, T.V. Krutskikh, S.M. Gubar, V.A. Georgiyants, IR-spectroscopy research into the structure of products of interaction between metronidazole and metal salts, Der Pharma Chem. 8 (2016) 148–154.
[55] F. Naseem, S.U. Shah, S.A. Rashid, A. Farid, M. Almehmadi, S. Alghamdi, Metronidazole based floating bioadhesive drug delivery system for potential eradication of H. pylori: preparation and in vitro characterization, Polymers 14 (2022) 1–23, https://doi.org/10.3390/polym14030519.
[56] S.V. Kumar, S.P. Kumar, D. Rupesh, K. Nitin, Journal of chemical and pharmaceutical research preparations, J. Chem. Pharm. Res. 3 (2011) 675–684.
[57] I. Kaur, S. Agnihotri, D. Goyal, Fabrication of chitosan – alginate nanospheres for controlled release of cartap hydrochloride, Nanotechnology 2 (2021), 025701, https://doi.org/10.1088/1361-6528/ac2d4c.
[58] E.L. Mogilevskaya, T.A. Akopova, A.N. Zelenetskii, A.N. Ozerin, The crystal structure of chitin and chitosan, Polym. Sci. - Ser. A. 48 (2006) 116–123, https://doi.org/10.1134/S0965545X06020039.
[59] M. Miya, Dependence on the preparation procedure of the polymorphism and crystallinity of chitosan membranes, Biosci. Biotechnol. Biochem. 56 (1992) 858–862, https://doi.org/10.1271/bbb.56.858.
[60] H.A. Kader Sabbagh, S.H. Hussein-Al-Ali, M.Z. Hussein, Z. Abudayeh, R. Ayoub, S.M. Abudoleh, A statistical study on the development of metronidazole-chitosan-alginate nanocomposite formulation using the full factorial design, Polymers 12 (2020), https://doi.org/10.3390/POLYM12040772.
[61] H.A.K. Sabbagh, Z. Abudayeh, S.M. Abudoleh, J.A. Alkrad, M.Z. Hussein, S.H. Hussein-Al-Ali, Application of multiple regression analysis in optimization of metronidazole-chitosan nanoparticles, J. Polym. Res. 26 (2019), https://doi.org/10.1007/s10965-019-1854-x.
[62] M. Gierszewska, J. Ostrowska-czubenko, E. Chrzanowska, pH-responsive chitosan/alginate polyelectrolyte complex membranes reinforced by tripolyphosphate, Eur. Polym. J. 101 (2018) 282–290, https://doi.org/10.1016/j.eurpolymj.2018.02.031.
[63] L. Wang, L. Sun, Z. Gu, W. Li, L. Guo, S. Ma, L. Guo, W. Zhang, B. Han, J. Chang, Bioactive Materials N -carboxymethyl chitosan/sodium alginate composite hydrogel loading plasmid DNA as a promising gene activated matrix for in-situ burn wound treatment, Bioact. Mater. 15 (2022) 330–342, https://doi.org/10.1016/j.bioactmat.2021.12.012.
[64] J.P. Soares, J.E. Santos, G.O. Chierice, E.T.G. Cavalheiro, Thermal behavior of alginic acid and its sodium salt, Eclét. Quím. 29 (2004) 57–63, https://doi.org/10.1590/s0100-46702004000200009.
[65] A. Pawlak, M. Mucha, Thermogravimetric and FTIR studies of chitosan blends, Thermochim. Acta 396 (2003) 153–166, https://doi.org/10.1016/S0040-6031(02)00523-3.
[66] A. Singh, A.K. Kar, D. Singh, R. Verma, N. Shraogi, Composite hydrogel beads as carrier for controlled release of Imidacloprid towards sustainable pest control, Chem. Eng. J. 427 (2022), 131215, https://doi.org/10.1016/j.cej.2021.131215.
[67] D. Kulig, A. Zimoch-Korzycka, A. Jarmoluk, K. Marycz, Study on alginate-chitosan complex formed with different polymers ratio, Polymers 8 (2016) 1–17, https://doi.org/10.3390/polym8050167.
[68] S.M. Ibrahim, F.I. Abou El Fadl, A.A. El-Naggar, Preparation and characterization of crosslinked alginate-CMC beads for controlled release of nitrate salt, J. Radioanal. Nucl. Chem. 299 (2014) 1531–1537, https://doi.org/10.1007/s10967-013-2820-4.
[69] T. Wu, Y. Li, N. Shen, C. Yuan, Y. Hu, Preparation and characterization of calcium alginate-chitosan complexes loaded with lysozyme, J. Food Eng. 233 (2018) 109–116, https://doi.org/10.1016/j.jfoodeng.2018.03.020.
[70] L. Wei, C. Cai, J. Lin, L. Wang, X. Zhang, Degradation controllable biomaterials constructed from lysozyme-loaded Ca-alginate microparticle/chitosan composites, Polymer (Guildf) 52 (2011) 5139–5148, https://doi.org/10.1016/j.polymer.2011.09.006.
[71] C. Sharma, A.K. Dinda, P.D. Potdar, C.F. Chou, N.C. Mishra, Fabrication and characterization of novel nano-biocomposite scaffold of chitosan-gelatin-alginate-hydroxyapatite for bone tissue engineering, Mater. Sci. Eng. C 64 (2016) 416–427, https://doi.org/10.1016/j.msec.2016.03.060.
[72] J. Yang, J. Chen, D. Pan, Y. Wan, Z. Wang, PH-sensitive interpenetrating network hydrogels based on chitosan derivatives and alginate for oral drug delivery, Carbohydr. Polym. 92 (2013) 719–725, https://doi.org/10.1016/j.carbpol.2012.09.036.
[73] S. Kumar, M. Prasad, R. Rao, Topical delivery of clobetasol propionate loaded nanosponge hydrogel for effective treatment of psoriasis: formulation, physicochemical characterization, antipsoriatic potential and biochemical estimation, Mater. Sci. Eng. C 119 (2021), 111605, https://doi.org/10.1016/j.msec.2020.111605.
[74] J.O. Jeong, J.S. Park, E.J. Kim, S.I. Jeong, J.Y. Lee, Y.M. Lim, Preparation of radiation cross-linked poly(Acrylic acid) hydrogel containing metronidazole with enhanced antibacterial activity, Int. J. Mol. Sci. 21 (2020), https://doi.org/10.3390/ijms21010187.
[75] G. Netanel Liberman, G. Ochbaum, R. Bitton, S. Malis, Arad, Antimicrobial hydrogels composed of chitosan and sulfated polysaccharides of red microalgae, Polymer (Guildf) 215 (2021), 123353, https://doi.org/10.1016/j.polymer.2020.123353.
[76] R. Os, M, Food Microbiology and Safety Chitosan Polymer as Bioactive Coating and Film against Aspergillus niger Contamination 70 (2005) 100–104, https://doi.org/10.1111/j.1365-2621.2005.tb07098.x.
[77] X. Wu, Z. Tang, X. Liao, Z. Wang, H. Liu, Fabrication of chitosan@calcium alginate microspheres with porous core and compact shell, and application as a quick traumatic hemostat, Carbohydr. Polym. 247 (2020), 116669, https://doi.org/10.1016/j.carbpol.2020.116669.
[78] N. Arslan, Ö. Yilmaz, E. Demiray-Gürbüz, Importance of antimicrobial susceptibility testing for the management of eradication in Helicobacter pylori infection, World J. Gastroenterol. 23 (2017) 2854–2869, https://doi.org/10.3748/wjg.v23.i16.2854.